Unidirectional ripples in strained graphene nanoribbons with clamped edges at zero and finite temperatures

Julia A. Baimova,[1,2] Sergey V. Dmitriev,[1] Kun Zhou,[2] and Alexander V. Savin[3]

[1]*Institute for Metals Superplasticity Problems, Russian Academy of Science, Khalturin Street 39, Ufa 450001, Russia*

[2]*School of Mechanical and Aerospace Engineering, Nanyang Technological University, 50 Nanyang Avenue, Singapore 639798*

[3]*Semenov Institute of Chemical Physics, Russian Academy of Sciences, Kosygin Street 4, Moscow 119991, Russia*

(Received 29 March 2012; published 18 July 2012)

Molecular dynamics simulations based on many-body interatomic potentials are conducted to investigate the formation of unidirectional ripples in zigzag and armchair graphene nanoribbons with clamped edges under in-plane uniform strain. The ripple formation is found to be a result of buckling under in-plane membrane forces having compressive and tensile principle components. This study demonstrates that the amplitude and orientation of the unidirectional ripples can be controlled by a change in the components of the applied strain. The ripple wavelength is practically independent of the applied strain but increases with the increasing nanoribbon width. In the study of the temperature effect on strain-induced ripples it was found that with increase in temperature the degree of fluctuation of ripples increases. Ripples with larger formation energy are less affected by thermal fluctuations.

DOI: 10.1103/PhysRevB.86.035427 PACS number(s): 05.45.Yv, 63.20.−e

I. INTRODUCTION

Graphene is a carbon polymorph that appears in the form of a two-dimensional honeycomb lattice, with each atom having three nearest neighbors. Recently, the remarkable physical, mechanical, chemical, and optical properties of graphene have attracted enormous attention of researchers to implement them in many applications such as graphene-based electronics,[1,2] optics,[2] photovoltaics,[3] spintronics,[4] hydrogen storage,[5] and composite materials,[6] to name a few.

Graphene has a record-breaking Young's modulus with respect to in-plane tension, but its flexural rigidity is practically zero. This feature means that graphene is very easy to bend and many researchers discuss how to introduce ripples or wrinkles in graphene sheets in a controllable fashion and how to use such corrugations.[7–23] In fact, wrinkling is a very general physical phenomenon demonstrated by thin sheets and membranes.[24,25]

One- or two-dimensional ripples can strongly influence electronic properties of graphene by inducing effective magnetic fields and changing local potentials.[10,11,20] Corrugations and strain present in most of the samples give rise to a space-dependent Fermi velocity.[21] It has been reported that graphene can loose its plane shape under in-plane shear[7] or applied uniaxial stress,[8–10] because of the interaction with a substrate,[11] due to internal or thermally induced stresses,[12] due to thermal fluctuations,[13] or under nanoindentation.[14] Wrinkles can form in graphene on soft substrates.[19] Elastic buckling of graphene under compressive loads has been investigated in the frame of the molecular structural mechanics method.[26,27] Atomistic continuum modeling of graphene membranes has been performed.[28] For a freely suspended graphene the corrugations reach up to 1 nm over a lateral scale of 10–25 nm, so that surface normal deviation is about $\pm 5^{\circ}$.[15] The corrugations of graphene can be considerably reduced by mica substrates.[16] To the our best knowledge, a comprehensive numerical analysis of unidirectional ripples in graphene throughout a wide range of in-plane strain ($\varepsilon_{xx}, \varepsilon_{yy}, \varepsilon_{xy}$) has not been done.

In this study we consider graphene nanoribbons with clamped edges to demonstrate that one-dimensional ripples with controllable orientation, wavelength, and amplitude can be introduced by the application of in-plane strain and by changing the nanoribbon width. Our setup is close to the case of graphene freely suspended over a trench considered in the experimental[12,24] and theoretical[7,24] studies. Our analysis includes also the case of large strains, which is in line with the elastic strain engineering, a rapidly developing branch of materials science.[29] We thus study the possibility to introduce ripples in graphene subjected to a large elastic strain. A considerable change of interatomic distances and lattice symmetry at such a large elastic strain can result in the appearance of unusual mechanical, thermal, optical, electrical, and other properties.[30,31] The addition of ripples to the structure of strained graphene can further modify its properties.

The case of ripples with wavelength comparable to the interatomic distance is also analyzed in the present work and, for this reason, we do not use a continuum mechanics approach based on a homogenization technique, although in other cases such modeling can be very efficient.[7,10,14,18,26–28] Our atomistic approach also enabled us to take into account the temperature effect on the strain-induced ripples.

In this work, interactions between atoms are described by a standard set of interatomic potentials that take into account valent bonds and angles between valent bonds, as well as torsion angles. A detailed description of the choice of potential parameters for graphene is given in Ref. 32. This set of interatomic potentials was successfully used for solving different problems such as finding the stability range for a flat graphene sheet subjected to in-plane deformation,[22,33] the thermoconductivity of graphene stripes with rough edges,[32] the thermoconductivity of carbon nanotubes,[34] the properties of discrete breathers in carbon nanotubes[35] and in strained graphene,[36] and the vibrational modes localized at the graphene edges.[37,38]

The rest of the paper is organized as following. Section II outlines the simulation setup. In Sec. III, for the reader's convenience, we reproduce the stability region of an infinite, flat graphene sheet in the space of the in-plane strain components ($\varepsilon_{xx}, \varepsilon_{yy}, \varepsilon_{xy}$) and in the space of the membrane forces

(T_{xx},T_{yy},T_{xy}), reported in our recent works.[22,33] Section IV presents our main findings on the parameters of unidirectional ripples in strained graphene nanoribbons with clamped edges. The temperature effect on the strain-induced ripples in graphene nanoribbons is discussed in Sec. V. Finally, the conclusions are briefly given in Sec. VI.

II. SIMULATION DETAILS

The primitive cell of flat graphene defined by the translation vectors $\mathbf{a}_1$ and $\mathbf{a}_2$ contains two carbon atoms, each having three degrees of freedom, namely the components of the displacement vectors [see Fig. 1(a)]. Note that the x (y) axis is along the zigzag (armchair) direction. In Fig. 1(b), the reciprocal space of the graphene lattice is shown with the first Brillouin zone defined by the vectors $\mathbf{b}_1$ and $\mathbf{b}_2$. High-symmetry points and lines of the first Brillouin zone are denoted by the capital Greek letters.

Let us denote the valent bond length in the unstrained graphene as $\rho_0 = 1.418$ Å, then the equilibrium lattice parameter is $a = |\mathbf{a}_1| = |\mathbf{a}_2| = \sqrt{3}\rho_0$. The atoms of graphene are numbered by the three indices m,n,k and their positions in unstrained graphene are defined by the radius vectors $\mathbf{R}_{m,n,k} = m\mathbf{a}_1 + n\mathbf{a}_2 + \mathbf{s}_k$, where the integers m,n give the primitive cell number and $k = 1,2$ numbers the atoms in a primitive cell. Primitive cell translation vectors can be taken as $\mathbf{a}_1 = a(1,0)$ and $\mathbf{a}_2 = (a/2)(1,\sqrt{3})$, and the sublattice shift vectors as $\mathbf{s}_1 = (0,0)$ and $\mathbf{s}_2 = (a/2,a/2\sqrt{3})$ [see Fig. 1(a)]. We subject graphene lattice to the in-plane strain with the components ε_{xx}, ε_{yy}, and ε_{xy}. The equilibrium positions of atoms in uniformly strained graphene are $\mathbf{r}^0_{m,n,k} = m\mathbf{p}_1 + n\mathbf{p}_2 + \mathbf{q}_k$. Translation vectors of the deformed primitive cell are $\mathbf{p}_1 = \mathbf{a}_1 + \mathbf{a}_1\mathbf{H}$ and $\mathbf{p}_2 = \mathbf{a}_2 + \mathbf{a}_2\mathbf{H}$, where the matrix

$$\mathbf{H} = \begin{pmatrix} h_{11} & h_{12} \\ h_{21} & h_{22} \end{pmatrix} = \begin{pmatrix} \varepsilon_{xx} & \varepsilon_{xy}/2 \\ \varepsilon_{xy}/2 & \varepsilon_{yy} \end{pmatrix}.$$

In the uniformly strained lattice the shift vector of the first sublattice can always be taken as $\mathbf{q}_1 = \mathbf{s}_1 = \mathbf{0}$, but the shift vector of the second sublattice, $\mathbf{q}_2$, should be found by minimizing the potential energy of the crystal with respect to its two in-plane components. The vector $\mathbf{q}_2^{(1)} = \mathbf{s}_2 + \mathbf{s}_2\mathbf{H}$ can be recommended as the first approximation. Note that such equilibrium flat configuration can be stable or unstable.

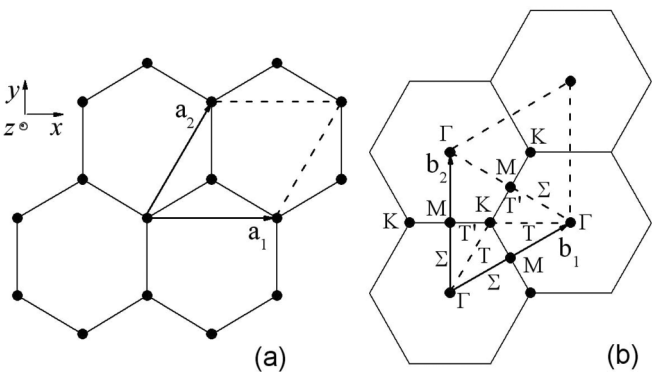

FIG. 1. (a) The primitive cell of flat graphene, defined by the translation vectors $\mathbf{a}_1$ and $\mathbf{a}_2$, contains two carbon atoms. (b) Reciprocal lattice of graphene with the first Brillouin zone defined by the vectors $\mathbf{b}_1$ and $\mathbf{b}_2$. The high-symmetry points and lines of the first Brillouin zone are denoted by the capital Greek letters.

In Refs. 22 and 33, the stability analysis of an infinite, flat graphene sheet under in-plane stain has been performed by calculating the frequencies of phonon modes, using the methodology presented, e.g., in Refs. 39 and 40. The flat shape of the infinite graphene sheet is stable if there are no negative eigenvalues ω^2 in the phonon spectrum throughout the first Brillouin zone.

Zigzag (armchair) nanoribbons in the simulations have edges along the x (y) axis. Clamped boundary conditions are used along the edges of the nanoribbons, while periodic conditions are employed along the direction normal to the edges.

The nanoribbon width is conveniently defined by the number of primitive cells N along the y (x) direction for the zigzag (armchair) nanoribbons. The actual width of the nanoribbon depends on N and on the applied elastic strain and can be calculated as $Na(\sqrt{3}/2)(1+\varepsilon_{yy})$ for the zigzag nanoribbon and $Na(1+\varepsilon_{xx})$ for the armchair nanoribbon. The nanoribbon length is defined by the number of primitive cells M along the x (y) direction for the zigzag (armchair) nanoribbons. The actual length of the nanoribbon can be calculated as $Ma(1+\varepsilon_{xx})$ for the zigzag nanoribbon and $Ma(\sqrt{3}/2)(1+\varepsilon_{yy})$ for the armchair nanoribbon.

Zigzag and armchair graphene nanoribbons subjected to in-plane uniform strain with components $(\varepsilon_{xx},\varepsilon_{yy},\varepsilon_{xy})$ were then relaxed to find the minimum-energy shape starting from the equilibrium plane structure slightly perturbed by out-of-plane displacements of order 10^{-4} Å. The initial velocities of all atoms were equal to zero. If the flat structure of graphene is stable, the perturbations disappear as a result of relaxation. If it is unstable, the nanoribbon either fractures or evolves to a shape with out-of-plane displacements of atoms. It is noted that the relaxation was carried out by means of molecular dynamics with a viscosity term introduced into the equations of atomic motion. The value of the viscosity coefficient was optimized to speed up the relaxation process.

The temperature effect on the nanoribbon ripples was studied. Temperature was introduced by setting the initial conditions in the form of the sum of all linear vibration modes whose total number is equal to the number of degrees of freedom of the system. The amplitudes of the modes were chosen so that they have equal energy and the total energy of the system is equal to a desired value. The initial phases of the modes are random numbers homogeneously distributed in the range from 0 to 2π. Such initial conditions mimic the system close to thermal equilibrium. Temperature can be calculated as

$$T = \frac{2}{3}\frac{\overline{K}}{k_B}, \tag{1}$$

where $\overline{K}$ is the averaged kinetic energy per atom and k_B is the Boltzmann constant and given as $k_B = 8.617 \times 10^{-5}$. The constancy of the temperature was controlled by the Nose-Hoover thermostat.[41]

III. STABILITY REGION OF FLAT GRAPHENE

The stability region of flat graphene is shown in Fig. 2(a) in the space of the in-plane strain components $(\varepsilon_{xx}, \varepsilon_{yy}, \varepsilon_{xy})$ as a set of sections by the planes $\varepsilon_{xy} = \text{const}$ projected on the

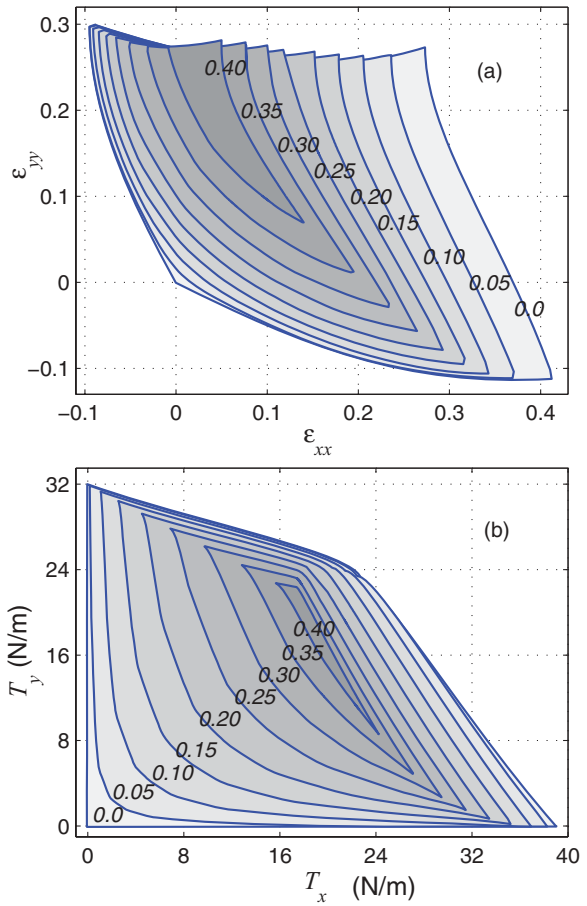

FIG. 2. (Color online) (a) The stability region of flat graphene in the space of the in-plane strain components (ε_{xx}, ε_{yy}, ε_{xy}) shown as the set of sections by the planes ε_{xy} = const (indicated for each section). (b) The membrane forces T_x and T_y calculated on the lines shown in (a).

plane (ε_{xx}, ε_{yy}).[22,33] The corresponding values of ε_{xy} are indicated for each section. Note that for the chosen coordinate system the sign of ε_{xy} is not important. We have calculated the values of membrane forces T_x, T_y, and T_{xy} on the borders of the stability region. In Fig. 2(b) the membrane forces T_x and T_y are given for the points on the lines shown in Fig. 2(a). Assuming that the graphene sheet has thickness h, the stress components can be calculated as $\sigma = T/h$. Often the interlayer distance in graphite, $h = 3.34$ Å, is taken as the graphene thickness.

For given T_x, T_y, and T_{xy} one can calculate the components of the principal membrane forces T_1 and T_2 and the orientation angles of the principal axes θ as follows:

$$T_1 = \frac{T_x + T_y}{2} + \frac{1}{2}\sqrt{(T_x - T_y)^2 + 4T_{xy}^2},$$
$$T_2 = \frac{T_x + T_y}{2} - \frac{1}{2}\sqrt{(T_x - T_y)^2 + 4T_{xy}^2}, \qquad (2)$$
$$\tan 2\theta = \frac{2T_{xy}}{T_x - T_y}.$$

Inside the stability region of flat graphene (Fig. 2) ripples cannot form. If the border of the stability region is crossed from inside on an increase of T_x or/and T_y, then both principal membrane forces, T_1 and T_2, are positive and fracture in graphene takes place rather than formation of ripples. If it is crossed from inside on a decrease of T_x or/and T_y, then T_1 or T_2 or both are negative and buckling in graphene occurs. In the present study we are interested in the case with one negative and one positive principal membrane force ($T_1 T_2 < 0$), when unidirectional ripples can form.

The above results of the stability analysis of an infinite flat graphene sheet can be modified for graphene nanoribbons by the effect of boundary conditions. One can expect that the stability region for nanoribbons with clamped edges could be wider than for an infinite sheet because typically constraints increase the stability of a system. This conjecture will be validated in the following section.

IV. STRAIN-INDUCED UNIDIRECTIONAL RIPPLES IN GRAPHENE NANORIBBONS

As discussed, the formation condition of unidirectional ripples in in-plane strained graphene is that in the equilibrium flat state one of the principal membrane forces should be negative and another one positive, i.e., $T_1 T_2 < 0$. In Fig. 3, on the plane (ε_{xx},ε_{yy}), we plot regions with different combinations of signs of principal membrane forces for the cases (a) $\varepsilon_{xy} = 0$, (b) $\varepsilon_{xy} = 0.1$, (c) $\varepsilon_{xy} = 0.2$, and (d) $\varepsilon_{xy} = 0.3$. It should be pointed out that the components of the membrane forces were

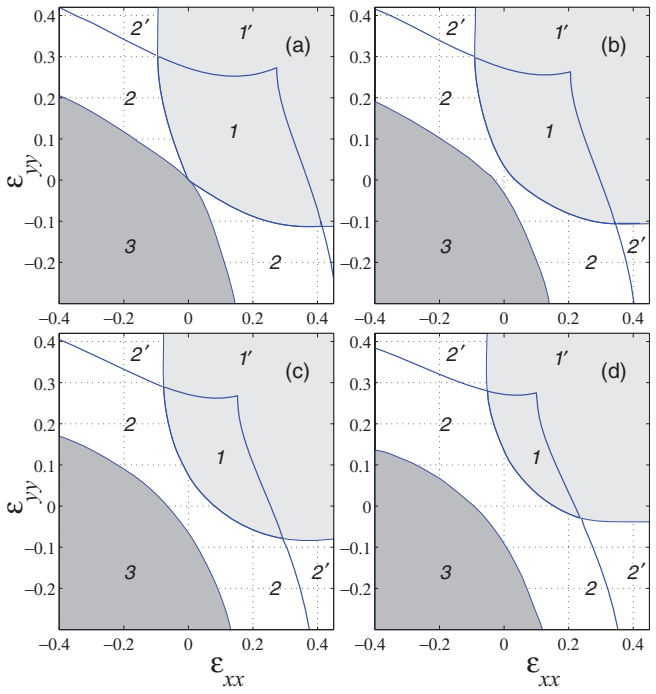

FIG. 3. (Color online) Regions of the (ε_{xx},ε_{yy}) plane with different signs of principal membrane forces for (a) $\varepsilon_{xy} = 0$, (b) $\varepsilon_{xy} = 0.1$, (c) $\varepsilon_{xy} = 0.2$, and (d) $\varepsilon_{xy} = 0.3$. In the light gray region $T_1 > 0$ and $T_2 > 0$. In the subregion 1 flat graphene is stable, while in the subregion 1′ fracture of graphene takes place. In the dark gray region 3 the flat graphene sheet is under compression in both principal directions, $T_1 < 0$, $T_2 < 0$. In the white region one of the principal membrane forces is positive and another one negative, $T_1 T_2 < 0$. In the subregion 2′ the tensile principal stress is too large and fracture of graphene takes place, while in the subregion 2 stable unidirectional ripples can form.

calculated for the (stable or unstable) equilibrium flat graphene subjected to corresponding uniform in-plane strain. In the region shown in light gray, $T_1 > 0$ and $T_2 > 0$ and ripples cannot form. In the subregion 1 flat graphene is stable [cf. Fig. 2(a)], while in the subregion $1'$ fracture of graphene takes place. Dark gray color shows the region 3 with $T_1 < 0$ and $T_2 < 0$. We do not study ripples in this region because they can be non-unidirectional. In the white region one of the principal membrane forces is positive and another one negative, $T_1 T_2 < 0$. In the subregion $2'$ the tensile principal membrane force is too large and fracture of graphene takes place, while in the subregion 2 stable unidirectional ripples can form.

Thus, it is concluded that stable unidirectional ripples can form in the white regions 2 of Fig. 3. Let us study the geometry of ripples in these regions. There are three main ripple parameters: orientation angle θ, amplitude, and wavelength.

In Fig. 4 we show the expected orientations of ripples in the case (a) $\varepsilon_{xy} = 0$ and (b) $\varepsilon_{xy} = 0.1$ by plotting line segments oriented along the direction of the tensile principal membrane force. Normal to these line segments the principal membrane force is compressive. In (a) ripples can be oriented either along the armchair or along the zigzag direction. In (b) the orientation of ripples gradually changes from the armchair to the zigzag direction on a decrease of ε_{yy} and an increase of ε_{xx}.

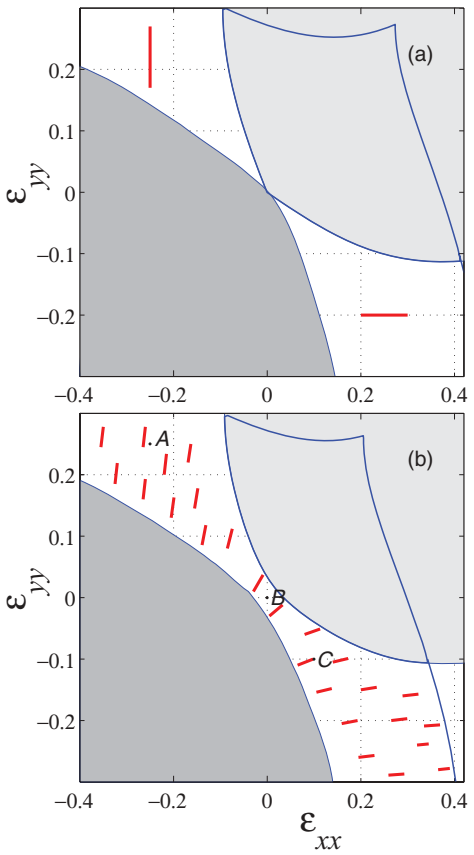

FIG. 4. (Color online) Expected orientations of ripples in uniformly strained nanoribbons in the case (a) $\varepsilon_{xy} = 0$ and (b) $\varepsilon_{xy} = 0.1$ shown by line segments oriented along the direction of tensile principal membrane force. Normal to these line segments the principal membrane force is compressive.

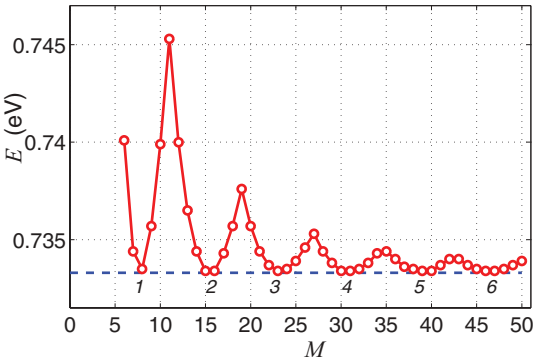

FIG. 5. (Color online) Potential energy per atom in the minimum-energy state for zigzag nanoribbon of width $N = 10$ as the function of nanoribbon length M. The nanoribbon is uniformly strained with $\varepsilon_{xx} = -0.23$, $\varepsilon_{yy} = 0.23$, and $\varepsilon_{xy} = 0$, and relaxed to a minimum-energy configuration taking into account not only in-plane but also out-of-plane displacements of atoms. When energy has a minimum, the nanoribbon length is close to an integer number of ripple wavelengths (indicated by the figures).

Results presented in Figs. 2–4 were obtained for an infinite flat graphene sheet from the analysis of its stability and from the calculation of the principal values and principal directions of the membrane forces. Now we turn to the discussion of the effect of boundary conditions considering zigzag and armchair nanoribbons with clamped edges.

We take the values of the strains within the region 2 of Fig. 3 where $T_1 T_2 < 0$ and find minimum-energy configuration for

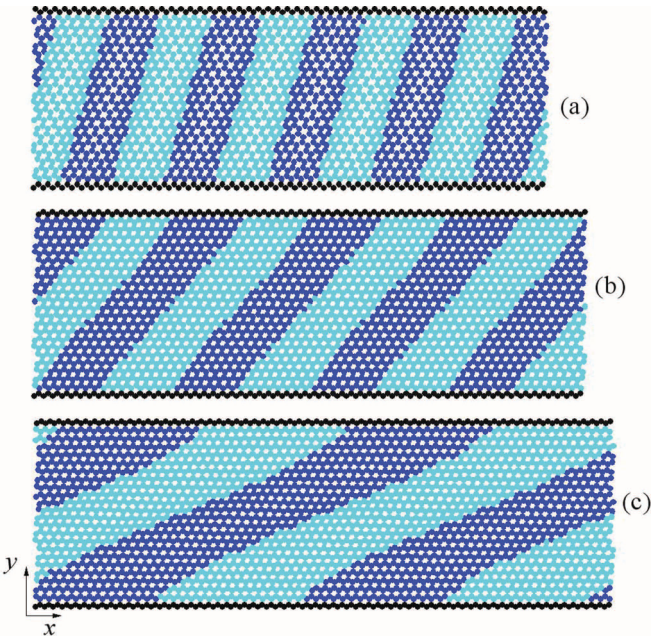

FIG. 6. (Color online) Examples of zigzag nanoribbons with stable ripples for the strain components $\varepsilon_{xy} = 0.1$ and (a) $\varepsilon_{xx} = -0.25$, $\varepsilon_{yy} = 0.25$; (b) $\varepsilon_{xx} = \varepsilon_{yy} = 0$; and (c) $\varepsilon_{xx} = 0.1$, $\varepsilon_{yy} = -0.1$. The corresponding points are marked in Fig. 4 by the letters A, B, and C, respectively. Dark and light carbon atoms have positive and negative out-of-plane displacements, respectively. Clamped atoms are shown in black.

nanoribbons taking into account not only in-plane but also out-of-plane degrees of freedom.

In Fig. 5 for the zigzag nanoribbon of width $N = 10$ we plot the potential energy per atom in the minimum-energy state as the function of the nanoribbon length M. In this case $\varepsilon_{xx} = -0.23$, $\varepsilon_{yy} = 0.23$, and $\varepsilon_{xy} = 0$. Recall that we use periodic boundary conditions for the ends of nanoribbons. When the energy E has a minimum, the nanoribbon length is close to an integer number of ripple wavelengths (indicated by the Figs. 1–6). From here one can estimate the ripple wavelength in an infinitely long nanoribbon to be $m = 46.5/6 = 7.75$ unit cells. The actual wavelength is $\lambda = ma(1 + \varepsilon_{xx}) = 14.7$ Å. In the following we always use this method to estimate the ripple wavelength.

In Figs. 6(a)–6(c), the examples of zigzag nanoribbons with stable ripples are given for the points in the strain space marked by the letters A, B, and C [Fig. 4(b)], respectively. Here the strain component $\varepsilon_{xy} = 0.1$ remains the same, while $\varepsilon_{xx} = -0.25$, $\varepsilon_{yy} = 0.25$ in (a), $\varepsilon_{xx} = \varepsilon_{yy} = 0$ in (b), and $\varepsilon_{xx} = 0.1$, $\varepsilon_{yy} = -0.1$ in (c). Dark and light carbon atoms have positive and negative out-of-plane displacements, respectively. Clamped atoms are shown in black. The zigzag nanoribbon has width $N = 20$ and the energy of the computational cell has a minimum when the nanoribbon length is (a) $M = 55$, (b) $M = 61$, and (c) $M = 65$. One can see that the orientations of ripples in the nanoribbon are in agreement with the orientations of the corresponding line segments in Fig. 4(b). Similar results were obtained for the armchair nanoribbons.

In Fig. 7, for (a) $\varepsilon_{xy} = 0$ and (b) $\varepsilon_{xy} = 0.1$, we show how the stability region of a flat nanoribbon expands with a decrease in its width N. The borders of stability in the regions $\varepsilon_{xx} < 0$, $\varepsilon_{yy} > 0$ ($\varepsilon_{xx} > 0$, $\varepsilon_{yy} < 0$) were obtained for the zigzag (armchair) nanoribbons. Values of N are indicated near the corresponding curves. The border of stability found for an infinite graphene sheet corresponds to $N = \infty$. It can be seen that for narrower nanoribbons the effect of stabilization of flat shape is stronger.

Let us now illustrate how the ripple amplitude and wavelength depend on strain. We take a zigzag nanoribbon of width $N = 15$ subjected to uniform strain with fixed components $\varepsilon_{yy} = 0.2$, $\varepsilon_{xy} = 0$ and vary ε_{xx}, thus moving along the horizontal dashed line shown in Fig. 7(a). The dashed line crosses the border of stability of a flat nanoribbon with $N = 15$ at $\varepsilon^*_{xx} = -0.122$ [the crossing point is marked with a circle in Fig. 7(a)]. The dependence of the ripple amplitude A on the strain component ε_{xx} is illustrated in Fig. 8(a). The

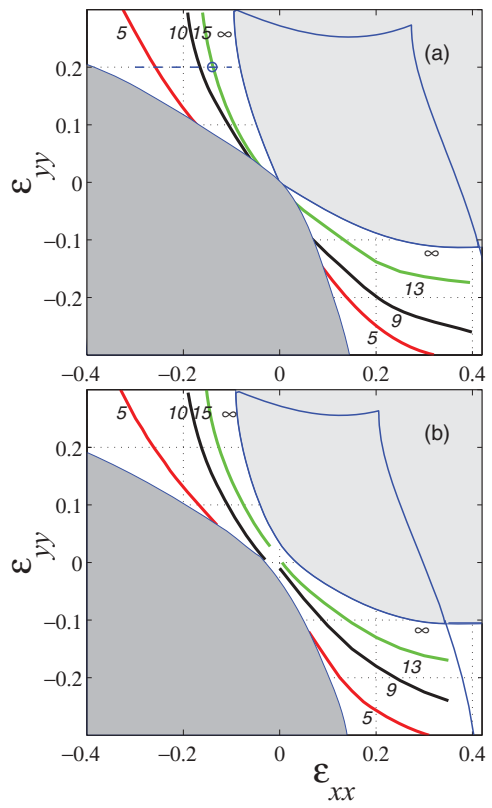

FIG. 7. (Color online) Borders of stability region of flat graphene nanoribbons of different width N for (a) $\varepsilon_{xy} = 0$ and (b) $\varepsilon_{xy} = 0.1$. The borders of stability in the regions $\varepsilon_{xx} < 0$, $\varepsilon_{yy} > 0$ ($\varepsilon_{xx} > 0$, $\varepsilon_{yy} < 0$) were obtained for the zigzag (armchair) nanoribbons. Figures near the curves indicate the corresponding values of N. The border of stability found for infinite graphene sheet corresponds to $N = \infty$.

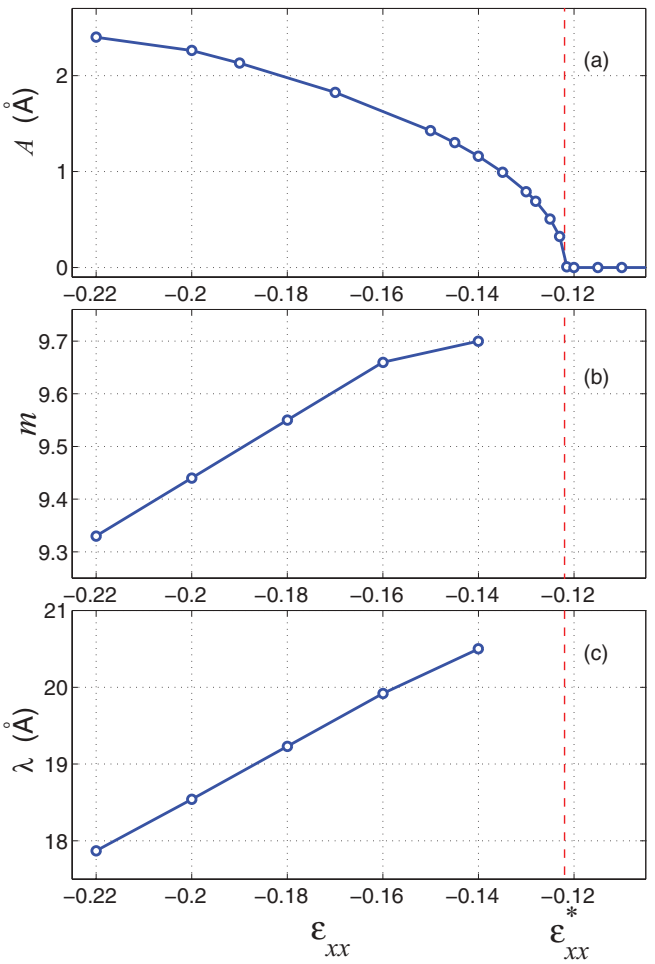

FIG. 8. (Color online) (a) Amplitude of ripples as the function of ε_{xx} for zigzag nanoribbon having width $N = 15$. (b), (c) Wavelength of the nanoribbon as the function of ε_{xx} measured in the number of primitive cells, m, and in angstroms, λ, respectively. Fixed components of strain are $\varepsilon_{yy} = 0.2$, $\varepsilon_{xy} = 0$.

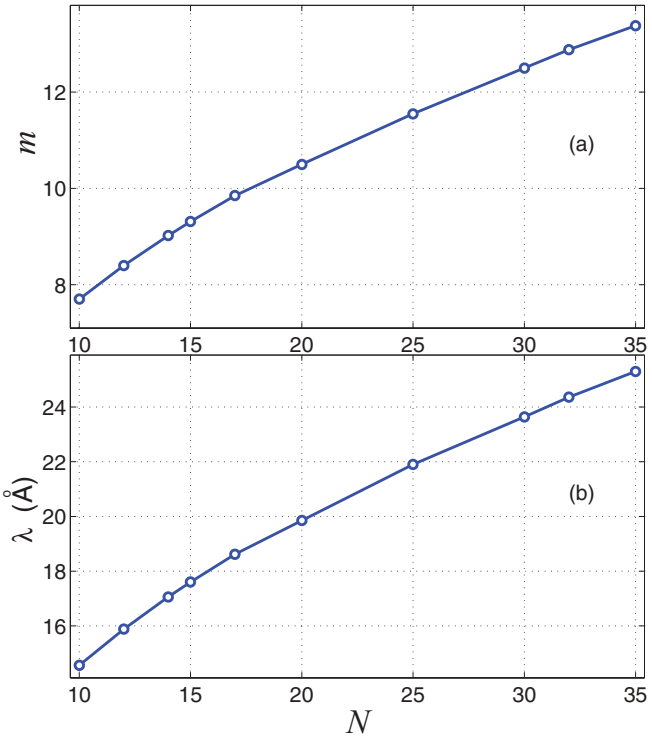

FIG. 9. (Color online) Wavelength of ripples as the function of nanoribbon width N for zigzag nanoribbons strained with $\varepsilon_{xx} = -0.23$, $\varepsilon_{yy} = 0.23$, $\varepsilon_{xy} = 0.0$. The wavelength in (a) is given in the number of primitive cells, m, while in (b) in angstrom, λ.

corresponding change in the ripple wavelength measured in the number of primitive cells, m, or in angstroms, λ, is shown in Figs. 8(b) and 8(c), respectively. It can be seen that $A = 0$ for $\varepsilon_{xx} > \varepsilon^*_{xx} = -0.122$, which means that the flat nanoribbon is stable in this region. In the region $\varepsilon_{xx} < \varepsilon^*_{xx}$ ripples exist with the amplitude increasing as $A \sim \sqrt{\varepsilon^*_{xx} - \varepsilon_{xx}}$. On the other hand, the ripple wavelength λ changes very slowly with strain. The results about the dependence of A and λ on strain obtained for the armchair nanoribbons are very similar.

In Fig. 9 for zigzag nanoribbons we show that the ripple wavelength measured (a) in the number of primitive cells, m, or (b) in angstroms, λ, increases with an increase in its width N nonlinearly for $N < 30$ and for larger N the increase is almost linear. In this example we take $\varepsilon_{xx} = -0.23$, $\varepsilon_{yy} = 0.23$, and $\varepsilon_{xy} = 0.0$. A similar linear dependence of the ripple wavelength on the nanoribbon width was found for the armchair nanoribbons.

V. TEMPERATURE EFFECT

The effects of temperature on the strain-induced ripples in zigzag nanoribbons having width of $N = 20$ periodic cells is considered for the following three strain states: (i) $\varepsilon_{xx} = -\varepsilon_{yy} = -0.05$, (ii) $\varepsilon_{xx} = -\varepsilon_{yy} = -0.10$, and (iii) $\varepsilon_{xx} = -\varepsilon_{yy} = -0.25$, with shear strain $\varepsilon_{xy} = 0.1$ in all cases.

We first describe parameters of equilibrium ripples at $T = 0$ K for the three cases giving the amplitude A; the orientation angle α; the wavelength λ; and the ripple formation potential energy per atom, $E = E_0 - E_r$, where E_0 is the potential energy per atom of the flat uniformly strained nanoribbon and E_r is the potential energy per atom of the relaxed nanoribbon with ripples: (i) $A = 1.72$ Å, $\alpha = 62°$, $\lambda = 15$ periodic cells, and $E = 0.0037$ eV; (ii) $A = 1.74$ Å, $\alpha = 71°$, $\lambda = 11$ periodic cells, and $E = 0.0123$ eV; and (iii) $A = 2.97$ Å, $\alpha = 80°$, $\lambda = 11$ periodic cells, and $E = 0.1123$ eV. The relaxed nanoribbons at 0 K for the cases (i)–(iii) are shown in Fig. 10(a), Fig. 10(d), and Fig. 6(a), respectively.

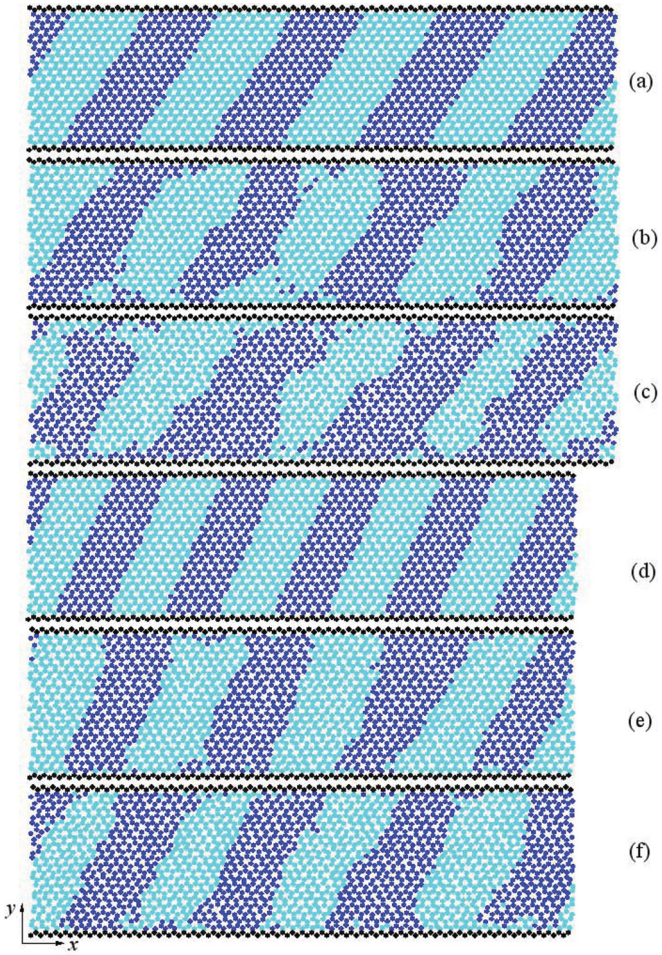

FIG. 10. (Color online) (a)–(c) Ripples in a zigzag graphene nanoribbon having width $N = 20$ subjected to the strain $\varepsilon_{xx} = -\varepsilon_{yy} = -0.05$, $\varepsilon_{xy} = 0.1$ at $T = 0$ K, $T = 1500$ K, and $T = 2500$ K, respectively. (d)–(f) Same as in (a)–(c), but for $\varepsilon_{xx} = -\varepsilon_{yy} = -0.1$. Dark and light carbon atoms have positive and negative out-of-plane displacements, respectively. Clamped atoms are shown in black.

The effect of temperature on the nanoribbon ripples in the case (i) can be seen from the snapshots (at $t = 100$ ps) presented in Fig. 10 with (a) for $T = 0$ K, (b) for $T = 1500$ K, and (c) for $T = 2500$ K. The same for the case (ii) is presented in Fig. 10 with (d) for $T = 0$ K, (e) for $T = 1500$ K, and (f) for $T = 2500$ K. It can be seen that in the case (i) the ripples are fluctuated by temperature stronger than those in the case (ii). This can be easily understood because the ripple formation energy in the case (ii) is more than three times larger than in the case (i). Note that in the case (ii) the ripples' wavelength changes from $\lambda = 11$ periodic cells at 0 K to

$\lambda = 55/4 = 13.75$ periodic cells at both 1500 and 2500 K [see Figs. 10(d)–10(f)]. This can be explained by the possibility of thermally activated transition from the structure corresponding to the global minimum of the potential energy to a metastable structure. It is worth pointing out that the melting temperature of unstrained graphene was calculated to be $T_m = 4900$ K.[42]

In the case (iii), in the three numerical runs with different random initial conditions corresponding to $T = 700$ K, fracture of the nanoribbon took place at $t = 53$, 68, and 109 ps. It should be pointed out that, at such a relatively low temperature, before fracture the ripples are only slightly affected by thermal fluctuations because the ripple formation energy in the case (iii) is much larger than in the cases (i) and (ii). The thermally activated fracture takes place because in the case (iii) rather large tensile strain is applied to the nanoribbon along the y axis. Thermal fluctuations result in breaking of a single interatomic bond oriented along the y axis followed by a rapid crack propagation along the x axis. In all three considered cases, the nanoribbon and the strain-induced ripples are robust enough to survive room temperature. The effect of temperature on the ripples was also studied for armchair nanoribbons. No new qualitative effects were observed as compared to those for zigzag nanoribbons.

VI. CONCLUSIONS

We have carried out an atomistic study of unidirectional ripples in graphene nanoribbons with clamped edges. The ripples appear as a result of buckling in flat graphene nanoribbons subjected to uniform in-plane strain $(\varepsilon_{xx}, \varepsilon_{yy}, \varepsilon_{xy})$ under the condition that one of principal membrane forces, T_1 and T_2, is positive and another one is negative. We have found the portion of $(\varepsilon_{xx}, \varepsilon_{yy}, \varepsilon_{xy})$ space where the necessary condition of existence of unidirectional ripples, $T_1 T_2 < 0$, is satisfied, and have demonstrated that clamped boundary conditions have stabilizing effect, which is stronger for narrower nanoribbons. Ripples are oriented along the positive principal membrane force because in the normal direction acts a compressive principal membrane force. The wavelength of ripples weakly depends on strain but it is almost proportional to the nanoribbon width for $N > 30$. The ripple amplitude increases as $A \sim \sqrt{\varepsilon^* - \varepsilon}$, where ε^* is a bifurcation point in the strain space and ε is the distance from this point.

In the study of the temperature effect on strain-induced ripples in zigzag nanoribbons the following effects were observed. With increase in temperature the degree of fluctuation of ripples increases. Ripples with larger formation energy E are less affected by thermal fluctuations. The ripple wavelength can be changed as a result of thermally activated transition from the structure corresponding to the global minimum of the potential energy to a metastable structure. For the nanoribbons subjected to large tensile strain, even at relatively low temperatures, thermal fluctuations can result in the breaking of an atomic bond followed by crack propagation and fracture of the nanoribbon. In the three strain states considered in the present study, the nanoribbon and the strain-induced ripples are robust enough to survive room temperature.

No qualitative difference was found between the parameters of ripples in zigzag and armchair nanoribbons.

Our results demonstrate that the parameters of unidirectional strain-induced ripples in graphene nanoribbons with clamped edges can be easily controlled by changing the strain components and nanoribbon width.

ACKNOWLEDGMENTS

S.V.D. and J.A.B. acknowledge financial support from Russian Foundation for Basic Research (Grant No. 11-08-97057-p-povolzhie-a); K.Z. and J.A.B. acknowledge the TIER 1 grant from the Ministry of Education, Singapore (Grant No. RG 56/11).

[1] A. K. Geim and K. S. Novoselov, Nat. Mater. **6**, 183 (2007).
[2] C. Soldano, A. Mahmood, and E. Dujardin, Carbon **48**, 2127 (2010).
[3] R. Won, Nature Photonics **4**, 411 (2010); X. Li, H. Zhu, K. Wang, A. Cao, J. Wei, C. Li, Y. Jia, Z. Li, X. Li, and D. Wu, Adv. Mater. **22**, 2743 (2010); C. C. Chen, M. Aykol, C. C. Chang, A. F. J. Levi, and S. B. Cronin, Nano Lett. **11**, 1863 (2011); K. Wu, W. Quan, H. Yu, H. Zhao, and S. Chen, Appl. Surf. Sci. **257**, 7714 (2011).
[4] N. Tombros, C. Jozsa, M. Popinciuc, H. T. Jonkman, and B. J. van Wees, Nature (London) **448**, 571 (2007).
[5] D. C. Elias, R. R. Nair, T. M. G. Mohiuddin, S. V. Morozov, P. Blake, M. P. Halsall, A. C. Ferrari, D. W. Boukhvalov, M. I. Katsnelson, A. K. G. Heim, and K. S. Novoselov, Science **323**, 610 (2009); J. O. Sofo, A. S. Chaudhari, and G. D. Barber, Phys. Rev. B **75**, 153401 (2007).
[6] S. Stankovich, D. A. Dikin, G. H. B. Dommett, K. M. Kohlhaas, E. J. Zimney, E. A. Stach, R. D. Piner, S. T. Nguyen, and R. S. Ruoff, Nature (London) **442**, 282 (2006).
[7] W. H. Duan, K. Gong, and Q. Wang, Carbon **49**, 3107 (2011).
[8] M. Neek-Amal and F. M. Peeters, Phys. Rev. B **82**, 085432 (2010).
[9] Z. F. Wang, Y. Zhang, and F. Liu, Phys. Rev. B **83**, 041403(R) (2011).
[10] F. Guinea, B. Horovitz, and P. Le Doussal, Solid State Commun. **149**, 1140 (2009).
[11] R. Miranda and A. L. Vazquez de Parga, Nat. Nanotechnol. **4**, 549 (2009).
[12] W. Bao, F. Miao, Z. Chen, H. Zhang, W. Jang, C. Dames, and C. N. Lau, Nat. Nanotechnol. **4**, 562 (2009).
[13] A. Fasolino, J. H. Los, and M. I. Katsnelson, Nat. Mater. **6**, 858 (2007).
[14] A. J. Gil, S. Adhikari, F. Scarpa, and J. Bonet, J. Phys.: Condens. Matter **22**, 145301 (2010).
[15] J. C. Meyer, A. K. Geim, M. I. Katsnelson, K. S. Novoselov, T. J. Booth, and S. Roth, Nature (London) **446**, 60 (2007).
[16] C. H. Lui, L. Liu, K. F. Mak, G. W. Flynn, and T. F. Heinz, Nature (London) **462**, 339 (2009).
[17] V. M. Pereira, A. H. Castro Neto, H. Y. Liang, and L. Mahadevan, Phys. Rev. Lett. **105**, 156603 (2010).
[18] K. Iyakutti, V. J. Surya, K. Emelda, and Y. Kawazoe, Comput. Mater. Sci. **51**, 96 (2012).

[19]Z. Li, Z. Cheng, R. Wang, Q. Li, and Y. Fang, Nano Lett. **9**, 3599 (2009).
[20]I. I. Naumov and A. M. Bratkovsky, Phys. Rev. B **84**, 245444 (2011).
[21]F. de Juan, M. Sturla, and M. A. H. Vozmediano, Phys. Rev. Lett. **108**, 227205 (2012).
[22]S. V. Dmitriev, J. A. Baimova, A. V. Savin, and Yu. S. Kivshar, Comput. Mater. Sci. **53**, 194 (2012).
[23]J. A. Baimova, S. V. Dmitriev, and K. Zhou, Phys. Status Solidi B **249**, 1393 (2012).
[24]H. Vandeparre, M. Pineirua, F. Brau, B. Roman, J. Bico, C. Gay, W. Bao, C. N. Lau, P. M. Reis, and P. Damman, Phys. Rev. Lett. **106**, 224301 (2011).
[25]Y. Mei, S. Kiravittaya, S. Harazim, and O. G. Schmidt, Mater. Sci. Eng. **70**, 209 (2010).
[26]S. C. Pradhan and T. Murmu, Comput. Mater. Sci. **47**, 268 (2009).
[27]A. Sakhaee-Pour, Comput. Mater. Sci. **45**, 266 (2009).
[28]R. Larsson and K. Samadikhah, Comput. Mater. Sci. **50**, 1744 (2011).
[29]T. Hu and J. Li, Prog. Mater. Sci. **55**, 710 (2010).
[30]X. Li, K. Maute, M. L. Dunn, and R. Yang, Phys. Rev. B **81**, 245318 (2010).
[31]F. M. D. Pellegrino, G. G. N. Angilella, and R. Pucci, Phys. Rev. B **81**, 035411 (2010).
[32]A. V. Savin, Yu. S. Kivshar, and B. Hu, Phys. Rev. B **82**, 195422 (2010).
[33]S. V. Dmitriev, Y. A. Baimova, A. V. Savin, and Y. S. Kivshar, JETP Lett. **93**, 571 (2011).
[34]A. V. Savin, B. Hu, and Yu. S. Kivshar, Phys. Rev. B **80**, 195423 (2009).
[35]A. V. Savin and Yu. S. Kivshar, Europhys. Lett. **82**, 66002 (2008).
[36]L. Z. Khadeeva, S. V. Dmitriev, and Yu. S. Kivshar, JETP Lett. **94**, 539 (2011).
[37]A. V. Savin and Yu. S. Kivshar, Europhys. Lett. **89**, 46001 (2010).
[38]A. V. Savin and Yu. S. Kivshar, Phys. Rev. B **81**, 165418 (2010).
[39]S. V. Dmitriev, T. Kitamura, J. Li, Y. Umeno, K. Yashiro, and N. Yoshikawa, Acta Mater. **53**, 1215 (2005).
[40]S. V. Dmitriev, J. Li, N. Yoshikawa, and Y. Shibutani, Philos. Mag. **85**, 2177 (2005).
[41]S. Nose, J. Phys. Soc. Jpn. **70**, 75 (2001).
[42]K. V. Zakharchenko, A. Fasolino, J. H. Los, and M. I. Katsnelson, J. Phys.: Condens. Matter **23**, 202202 (2011).